Published in final edited form as:
Neurosurgery. 2010 February ; 66(2): 323–332. doi:10.1227/01.NEU.0000360379.95800.2F.

Transcranial MRI-guided focused ultrasound surgery of brain tumors: Initial findings in three patients

Nathan McDannold, Ph.D.[1,2], **Greg Clement, Ph.D.**[1,2], **Peter Black, M.D.**[1,3], **Ferenc Jolesz, M.D.**[1,2], and **Kullervo Hynynen, Ph.D.**[4,1]

[1] Brigham & Women's Hospital, Boston, MA, Department of Radiology

[2] Harvard Medical School, Boston, MA

[3] Brigham & Women's Hospital, Boston, MA, Department of Neurosurgery

[4] Department of Medical Biophysics, University of Toronto and Sunnybrook Health Sciences Centre, Toronto, Ontario, Canada

Abstract

Objective—This work evaluated the clinical feasibility of transcranial MRI-guided focused ultrasound surgery (TcMRgFUS).

Methods—In initial trials in three glioblastoma patients, multiple focused ultrasound exposures were applied up to maximum acoustic power available. Offline analysis of the MR temperature images evaluated the temperature changes at the focus and brain surface.

Instrumentation—The method combines a hemispherical phased array transducer and patient-specific treatment planning based on acoustic models with feedback control based on MR temperature imaging to overcome the effects of the skull and allow for controlled and precise thermal ablation in the brain.

Technical Development—TcMRgFUS offers a potential noninvasive alternative to surgical resection.

Results—We found that it was possible to focus an ultrasound beam transcranially into the brain and to visualize the heating with MR temperature imaging. While we were limited by the device power available at the time and thus appeared to not achieve thermal coagulation, extrapolation of the temperature measurements at the focus and on the brain surface suggests that thermal ablation will be possible with this device without overheating the brain surface, with some possible limitation on the treatment envelope.

Conclusion—While significant hurdles remain, these findings are a major step forward in producing a completely noninvasive alternative to surgical resection for brain disorders.

Please send correspondence to: Nathan McDannold Department of Radiology, Brigham and Women's Hospital 221 Longwood Ave. (LMRC, 521) Boston, MA 02115 Tel: (617) 278-0605 Fax: (617) 732-7450 njm@bwh.harvard.edu .

Statement justifying each author's involvement in the production of the manuscript.

All authors edited the manuscript

Nathan McDannold analyzed the data and wrote the manuscript.

Nathan McDannold, Greg Clement, and Kullervo Hynynen were the technical team for the study and were involved with all non-clinical aspects of the treatment and interpretation of the results.

Ferenc Jolesz was the neuroradiologist for the treatments and determined the treatment plan.

Peter Black was the neurosurgeon for these treatments and the primary investigator of the clinical trial.

Keywords

Ultrasonic Therapy; Ablation Techniques; Brain; Tumor; MRI

Introduction

Despite progress made in many cancer treatments, brain tumors remain an extraordinary challenge. Due to the inherent risks with associated surgical resection and radiotherapy, combined with the aggressiveness of many CNS tumors and the difficulty in delivering anticancer drugs to the brain, the prognosis for patients with many types of brain tumors remains grim. New and less invasive alternatives to existing procedures are desperately needed.

Thermal ablation has been pursued as an alternative to surgery for tumor therapy in several targets, including the brain (1,31,32). It can be used to destroy tumors with little or no effects to the surrounding tissue, producing immediate and localized thermal coagulation. It can be used along with, potentially synergistically with, radiotherapy or chemotherapy. Thermal ablation, which does not utilize ionizing radiation, can also be reapplied in the case of recurrence.

A completely noninvasive approach to thermal ablation that has been tested for more than sixty years has been focused ultrasound. An ultrasound beam can be precisely focused deep into soft tissue. High intensities, resulting in localized heating due to absorption of the acoustic wave, can be achieved in the focal zone without damaging the surrounding tissues. Since the first tests (34), focused ultrasound has been investigated for the treatment of brain disorders. Pioneering work by William and Francis Fry (5,19) and others (2,4,33,50,52) showed the huge potential of this technology in animal trials, and promising clinical treatments of neurological disorders were performed (22,40). Despite the early promise, the use of focused ultrasound, particularly in the brain, has not reached widespread use. The challenge has been due to two main obstacles: a lack of control of the procedure and the difficulty in applying ultrasound through the skull.

Improvements in medical imaging have led to a resurgence of interest in focused ultrasound in recent decades. Ultrasound imaging, which allows some ability to target the beam, and more significantly MRI, which allows for exquisite targeting and feedback control of the procedure with quantitative temperature imaging (29), has led to several focused ultrasound systems designed for a wide range of targets outside of the brain that have been tested in trials or are now approved for clinical use (8,44,48,53). MRI guidance has also been demonstrated for laser thermal ablation in the brain (30-32).

Despite these developments, the skull has been an obstacle for the use of focused ultrasound in the brain. In the first focused ultrasound trials (22,40), the ultrasound exposures ("sonications") were performed through a craniotomy, making a noninvasive procedure invasive and substantially less desirable. For this reason, only a few other clinical trials in the brain have been attempted (20,21,41-43).

Transcranial application of focused ultrasound has been prevented because of the interaction of the skull on the ultrasound propagation. Acoustic attenuation in bone, which is ~30-60 times higher than in soft tissue, causes rapid heating in the skull and limits the exposure levels that can be safely applied. We have proposed a solution to this problem, where a hemispherical transducer operating at a lower frequency is used to generate the ultrasound beam and the scalp is actively cooled (13,47). The lower ultrasound frequency reduces absorption in the skull, and the hemispherical design distributes the resulting bone heating over a large enough area to

prevent overheating. Its large geometric aperture also increases the gain of the transducer and permits sufficient focal intensity to allow for ablation even at lower frequencies. Simulations and experiments suggest that an optimal ultrasound frequency to balance the skull and focal heating is approximately 700 kHz (12), lower than the 1-4 MHz commonly used in other targets.

While lower frequency ultrasound and a hemisphere design can mitigate bone heating, the skull also has a huge effect on the beam propagation. It is sometimes possible to focus an ultrasound beam through some locations in the skull (18), but variations in skull shape and thickness make it impossible to achieve such focusing reliably without some sort of correction. These aberrations can be corrected using an array of a large number of transducers to tailor the beam propagation (26,49). With individual driving hardware for each element of this array, one can apply phase offsets to correct for delays in the wave propagation at each location in the skull. The patient-specific corrections required for each element of this phased array can be determined using acoustic simulations combined with the geometric and density information obtained from CT scans of the skull acquired before treatment (3,9). Phase offsets can also be used to steer the focal position electronically, and modification of the amplitude of each element can normalize the ultrasound intensity across the brain surface.

Based on extensive preclinical acoustic (9-13,16,26,47) and MRI (28,36,37,51) studies, a clinical prototype of a phased array transcranial MRI-guided focused ultrasound surgery (TcMRgFUS) device for thermal ablation was developed (15,25,27). Here we present initial technical results of this device from patient treatments, demonstrating the feasibility of focusing through the skull and measuring the temperature rise at the focus and on the brain surface using MRI. Detailed clinical findings will be presented at a later date at the completion of the study.

Materials and Methods

Patients

The treatments were approved by our local IRB, and we obtained informed consent. Three men (age: 47, 23, 34) with glioblastoma were treated with TcMRgFUS as part of a phase I clinical trial at our institution testing feasibility and safety. All three patients were treated with chemotherapy and radiation therapy before TcMRgFUS, and surgery was not offered as an option by the referring neurosurgeon. Inclusion criteria allowed treatment of adult patients (age 18-70 years) with either inoperable recurrent glioblastoma (grade IV on the ASTRO scale) or recurrent metastatic cancer to the brain with defined margins on contrast MRI. Eligibility requirements included limitations on tumor number, size and location, patient health, and on medical history. Patients unable to undergo an MRI exam, unable to communicate sensations to the treatment team during TcMRgFUS, with extensive changes to 30% or more of the skull or scalp from disease or prior surgery, with surgical clips or devices in the skull or brain, in unable to attend all study visits (i.e., life expectancy less than three months), with evidence of recent (less than two weeks before TcMRgFUS) hemorrhage, or who anticipated alternative treatments within 30 days were excluded from the trial. Before treatment, the head was shaved, and the patient lied supine on the treatment device, which was integrated into a standard MRI table. The patient's head was stabilized using a thermoplastic mask designed for radiotherapy (Med-Tec, USA) with minor mechanical adaptations to the patient interface. They were awake during the procedure, but under intravenous conscious sedation, and were instructed to inform the team if any pain was present during sonication. The patient, anesthesiologist, and the TcMRgFUS operator also had access to a button which when pressed would immediately stop any sonication in case of pain. Patient vitals signs were monitored throughout treatment by the anesthesiologist, who remained in the MRI room throughout the procedure. Core body temperature was maintained using a heated blanket (Bair Hugger model 750, Arizant, USA).

Device

The treatments were performed using the ExAblate 3000 TcMRgFUS system (InSightec, Haifa, Israel), which consists of a 30 cm diameter hemispherical 512 element phased array transducer operating at 670 kHz coupled with a 512-channel driving system, a treatment planning/MRI thermometry/dosimetry workstation, and a water cooling/circulation/degassing system. The system was integrated with a clinical 1.5T MRI unit (General Electric Medical Systems, Milwaukee, WI). The system allowed for individual control of the phase and amplitude for each element in the phased array. The maximum total acoustic power applied was 650 W during patient one, and increased to 800 W for patients two and three. The lower value for patient one resulted from a conservative software setting. Calibration of the device was supplied by the manufacturer. The width and length of the half intensity profile produced by the transducer in water were 2 and 4 mm, respectively. MR imaging was performed using the body coil.

The transducer was oriented on its side and was housed in a manually-operated positioning system with six degrees of freedom (xyz translation, three angles) that was integrated into a standard MRI table. This positioning system was used to place the geometric focus of the transducer to the center of the planned tumor target; additional focal steering was achieved using electronic steering via the phased array. The location and orientation of the transducer in the MRI space was monitored throughout treatment using four small MRI tracking coils embedded as part of the transducer housing. The 512 channel driving system was located inside the MRI room. A control computer and power supply, as well as the water circulation/ degassing/chilling system and the treatment planning/dosimetry workstation were located outside the room. Figure 1 shows a diagram of the system.

A circular flexible membrane was used to contain the water that filled the space between the transducer and the head. This membrane had a hole cut in it that was stretched around the patient's head. The hole was tight enough to prevent water from leaking out, but not so tight as to cut off blood flow to the scalp. The membrane's outer circumference was sealed to the outside face of the transducer. The water allowed for acoustic coupling of the ultrasound beam and cooled the scalp to reduce the risk of thermal damage resulting from skull heating. This water was chilled to 15-20°C and was circulated between sonications. Water temperature and pressure inside the transducer were monitored throughout treatment.

The treatment planning software was used to provide phase offsets to compensate for skull-induced beam aberrations based on CT scans showing the geometry and density of the skull. For each transducer elements with an angle between it and the skull surface less than 45°, an algorithm similar to that presented in Ref. (9) was used that to add a phase offset to correct for the effect of the bone. This offset was determined by the average thickness and density of the skull in the path of the element (10). For angles greater than or equal to 45°, total reflection was assumed (14) and the element was deactivated. The relationship between the density measured on the CT scan and the speed of sound was that found experimentally in ex vivo human skulls (10). The amplitude of each element was modulated to obtain an equal acoustic intensity on average at the brain surface.

TcMRgFUS Treatment

Before treatment, the patient received a CT scan (512×512 matrix, 1 mm slice thickness) that covered the entire skull and an MRI exam with contrast (Gadopentetate dimeglumine, Magnevist®, Berlex Laboratories, Wayne NJ; dose: 0.1 mmol/Kg) obtained with the patient in place in the device (without water). Axial, sagittal, and coronal T2-weighted fast spin echo (FSE) images and contrast-enhanced T1-weighted images were used to define the tumor volume for treatment planning. During this imaging session, the thermoplastic mask was fit to

the patient, and the position and angle of the transducer was set via the manual positioning system so the geometric focus was located in the center of the target volume and that the transducer beam path covered as large a surface area on the skull as possible. These images were used to prescribe a detailed treatment plan that was used on the following day. The different imaging sets were registered to each other and to the current MRI/transducer coordinates using volumetric registration algorithms developed as part of ExAblate 3000 software tools (7). The CT scan was used in acoustic models by the TcMRgFUS software to correct for ultrasound beam aberrations. It covered the entire head instead of only the portion for which the ultrasound beam passed to facilitate its registration with subsequent MR scans.

On treatment day, the patient and TcMRgFUS device were prepared as described above, and axial, sagittal, and coronal T2-weighted FSE images were acquired. These images were registered to the previously acquired CT and MR images, and the treatment plan was displayed (Figure 2). This registration was verified visually by the operator by displaying the skull (automatically segmented in the CT scan) as a colored overlay on the MRI scans. Registration errors were corrected using a graphical tool integrated in the planning software. The individual beam paths were also displayed on top of the images, allowing for any element to be deactivated if its path passed through unwanted locations, which in these patients were burr holes and sites of previous surgical resection. After this plan was completed, sonication began.

The acoustic power was slowly increased over several 20s sonications until focal heating was observed in MR temperature imaging (MRTI) to verify the target location within the tumor. After such verification, the acoustic power was increased further over additional 20 s sonications. The goal was to achieve a sufficient thermal dose (45) to achieve thermal coagulation, approximately 55°C peak temperature or 240 equivalent minutes at 43°C (TEM43) (39). However, as described below, we were limited by the device's maximum acoustic power level (650W in patient number one, 800W in patients two and three), and in patient number 3, pain.

For MRTI, phase-difference images of a fast spoiled gradient echo (FSPGR) sequence were obtained to estimate changes in the temperature-sensitive water proton resonant frequency (29). The following parameters were used for MRTI: TR/TE: 38/19 ms, flip angle: 30°, slice thickness: 3-5 mm, field of view: 28 cm, matrix (frequency×phase): 256×128, bandwidth: ±3.57 kHz, scan time: 5 s. A time-series of images in a single, user-defined plane were obtained before, during, and after each sonication. The scanner reconstructed complex image data needed to create these phase-difference images, which were converted to temperature maps by the treatment planning/thermometry workstation using a temperature sensitivity of −0.01 ppm/°C (23). Estimates of absolute temperatures assumed a 37°C baseline tissue temperature.

Post-treatment analysis

Post-treatment data analysis was performed by one author (NM) using software written in Matlab (version 7.4, The Mathworks, Natick, MA). The maximum temperature rise achieved at each visible focal hotspot was calculated and compared to the heating on the outer brain surface induced by ultrasound absorption in the skull. To combine the results of the different sonications, which were performed at different exposure levels, we normalized the temperature rise to the applied acoustic power – a valid assumption assuming linear acoustic propagation (24).

While the ultrasound intensity outside the focal region is expected to be insufficient to produce direct heating of brain tissue, the skull will heat appreciably due to high acoustic absorption and will as a result heat the brain surface. As skull-induced brain surface heating will be a major limiting safety factor for TcMRgFUS, the temperature changes in this area were carefully examined using the following procedure. First, the entire brain was manually segmented in the

magnitude FSPGR images used for the MRTI, excluding areas between the brain surface and skull containing cerebral spinal fluid. The outer brain surface within the transducer path was then identified. A range of thee or more consecutive temperature images were also identified near the end of the time-series of the MRTI where the brain surface temperature appeared reach a steady-state and that were free of phase artifacts that persisted after application of the correction scheme described below. These persistent artifacts were manifested by temporal jumps in temperature that were clearly inconsistent with expected heating. Brain surface heating was measured on coronal and sagittal images; axial images were excluded because the skull was not necessarily normal to the image plane, and partial volume effects could dominate. Temperature measurements within the skull were not possible because a lack of MR signal in bone.

Two procedures were used to quantify the brain surface heating. In the first, the overall mean surface heating was calculated in a two voxel wide strip at the brain surface. In the second, a conservative (worse-case) metric that attempted to take into account non-uniform heating was devised. The mean temperature rise of the hottest 5% of the voxels within 6-7 voxels (approximately 7 mm) of the outer brain surface was identified. To minimize bias to noise or artifacts unrelated to temperature, these voxels were identified on the averaged map of three or more images at the end of the MRTI time-series when the heating reached steady state, and the region defined by these voxels was extended by one voxel in every direction. These criteria were determined ad-hoc with an aim of including only the hottest voxels but with a sufficient number to average out noise or other temperature measurement artifacts, which were assumed to be randomly distributed around zero. Brain surface heating values quoted below are the average of three or more images where the temperature rise appeared to stabilize.

Phase instabilities in the MRTI were corrected in post-treatment analysis using non-heated brain areas. To define these areas, the segmentation of the brain surface was eroded at the edges by 6-7 voxels (approximately 7 mm) and a circular 1 cm region of interest (ROI) surrounding the focal target was excluded. Voxels within ventricles were also excluded because they had uncorrelated phase artifacts resulting from fluid flow presumably resulting from acoustic streaming. The phase-difference distribution in the remaining non-heated/non-ventricular voxels was then fit to a non-specific smooth surface using a regularized, piecewise linear (low order spline) surface model. The regularization is based on the Laplacian of the surface, and is used to penalize deviations from smoothness in the fitted surface. This surface fit of the artifact was then extrapolated into the heated regions at the focal point and outward to the brain surface and subtracted off. The ability of this method to correct for phase instabilities was tested by repeating this procedure in a separate one cm ROI in a non-heated area instead of the focal point and verifying that its average phase offset approached zero. We could not verify the correction algorithm in this way on regions at the brain surface because no images were obtained without potential heating. The noise level in the MRTI was found by calculating the average standard deviation in the non-heated ROI's used to test the correction scheme. Separate noise estimates were obtained for images acquired during and after sonication. The maximum temperature rises per W at the focus and on the brain surface were compared using an unpaired t-test. Differences between the two metrics for brain surface heating estimates were compared using a paired t-test.

Results

T2-weighted FSE images of the three patients within the TcMRgFUS device are shown in Figure 3. The location of the target tumors in the thalamus were relatively deep and central within the brain. The skull area that the acoustic beam was distributed over was calculated by the treatment planning workstation to be 284, 327, and 354 cm^2, for patients 1-3 respectively. The highest acoustic power level attempted in patient number one was 650 W, which was the

maximum value available for that treatment due to a conservative software setting. The maximum acoustic power available for the other patients was 800 W. This level was achieved in patient number two, but in patient three, sonication-related pain was reported at 650 W, and higher values were not tested. Pain related to the thermoplastic mask and neck support limited the treatment time available. Comparison of pre- and post-TcMRgFUS images showed that small patient motion (approximately 2-4 mm) occurred over the course of the treatment.

Focal heating was readily observed within the target tumor in MRTI during 3/12, 14/16, and 11/17 of the sonications delivered in patients 1-3, respectively. The overall maximum focal temperature achieved during a 20s sonication was approximately 51°C, near but not clearly above the threshold for thermal damage in the brain (37). Individually, the maximum temperature achieved was 42, 51, and 48°C, for patients 1-3, respectively. Changes resulting from treatment were not evident in the tumor, surrounding brain, or brain surface in post-TcMRgFUS MRI acquired immediately after the procedure. No skin burns were observed after treatment, and no skin pain was reported.

The resulting maximum estimated average acoustic intensity on the outer skull surface for the three patients was 2.8, 2.5, and 1.8 W/cm^2, respectively for the three patients. The maximum temperature rise in the hottest regions within 7 mm of the brain surface was 2.5, 3.8, and 2.4° C. This result represents a conservative estimate of brain surface heating that allowed for hotspots at discrete locations, but that was also potentially sensitive to bias. When considering all voxels within a two voxel wide strip at the edge of the brain surface, the maximum measured brain surface temperature rise resulting from skull heating was 0.9, 1.5, and 1.2°C. Overall, the temperature rise on the brain surface per average W/cm^2 on the outer skull surface (estimated by TcMRgFUS software) was 1.3 ± 0.3 and 0.5 ± 0.2 °C/W/cm^2, for the two metrics tested. Figure 4 shows examples of the focal and skull heating observed in the MRTI. No heating other than at the focus and on the brain surface was observed.

When normalizing all of the measurements to the applied acoustic power, the average ratio between the focal heating and that of the hottest voxels near the brain surface induced by skull heating was 4.0 ± 1.7; the mean ratio between the focal heating and that of the two voxel wide strip at the brain surface was 10.5 ± 5.5. The mean normalized temperature rise per watt (± S.D.) at the focus and at the brain surface (using both criteria) for all sonications are plotted in Figure 5. As expected, the focal temperature rise peaks at the end of the 20 s sonication and then cools in subsequent images, while the brain surface continues to heat past 20 s as the skull continues to heat the adjacent brain surface via thermal conduction. The peak temperature rise per acoustic W at the focus was significantly larger than that achieved on the brain surface ($P<0.01$). The peak brain surface temperature rise estimated using the hottest voxels was significantly larger ($P<0.01$) than that estimated using the two voxel wide strip at the edge of the brain.

Severe instabilities that were observed in the phase difference images used for MRTI (Figure 6A) were subtracted off by fitting the non-heated regions of the brain to a smooth surface (Figure 6B) and extrapolation (Figure 6C). The correction scheme appeared to robustly correct the phase artifacts, as evidenced by analysis of non-heated ROI's substituted for those used around the focus (Figure 6D). Before correction, the average root mean squared phase error in test locations was 1.9 ± 3.4°C; after correction, this value was 0.3 ± 0.2°C. The average standard deviation inside these non-heated ROI's, reflective of the image signal-to-noise ratio, was ±1.3 ± 0.4°C. It increased to ±1.6 ± 0.6°C during sonication. A signal void, presumably due to blood products from a prior biopsy, in a large part of the tumor in patient 3 limited the use of MRTI in that region (Figure 6E).

Discussion

The study has demonstrated for the first time that a therapeutic ultrasound beam can be focused in the brain noninvasively through the intact skull in patients. While sufficient power was not available to us to clearly achieve thermal coagulation and significant hurdles remain, these findings are a major step forward in producing a completely noninvasive alternative to surgical resection for brain disorders. As described below, based on these findings it appears that TcMRgFUS ablation of brain tumors will be feasible with this device. If this result is verified, a noninvasive alternative to surgical resection could be available to patients, potentially reducing side effects of surgery and providing a treatment options for patients with inoperable tumors. It could also provide an alternative to radiosurgery or a treatment option for patients with recurrence after radiotherapy.

These treatments were in patients with inoperable glioblastoma, which may not ultimately be the best clinical target for TcMRgFUS because of its infiltrative nature. This treatment is a noninvasive alternative to surgical resection. While it offers a major reduction in side-effects, it is known that surgery offers only limited improvement in survival for these patients. We anticipate that better targets for TcMRgFUS will be those for which surgical resection currently offers greater benefit, such as metastases or other tumors with well-defined margins, or benign tumors. One may ultimately be able to improve upon surgical resection with TcMRgFUS by taking advantage of synergistic effects of heat with radiation therapy or chemotherapy.

Extrapolation of the mean focal temperatures and a conservative estimate of skull-induced heating achieved during these treatments suggest that with sufficient power, one could achieve thermal coagulation at the focus without overheating the brain surface. For example, the average measurements at the focus suggest that to achieve a peak focal temperature of 55°C, which would be sufficient to produce thermal necrosis, would require approximately 1200 W of acoustic power for a 20 s sonication. At this value and assuming a baseline temperature of 37°C, our measurements suggest that the brain surface would heat to approximately 39-42°C, which is below the thermal damage threshold for the relatively short heating durations employed with TcMRgFUS. Other effects have been observed for low-level heating for longer heating durations, such as necrosis (35) and febrile seizures (6,17). One needs to consider the risk for such effects resulting from the cumulative thermal dose on the brain surface when multiple sonications are employed to treat a tumor volume.

The mean brain surface temperature per W/cm^2 on the brain surface was lower than measured in pre-clinical animal tests. In primate tests (27), the mean temperature elevation across the brain surface was 2.6 ± 0.2 °C per W/cm^2, with the hottest voxels giving an average value of 4.0 ± 0.2°C per W/cm^2. In similar pig experiments (36) the average brain surface heating was observed to be 2.2 ± 0.5 °C per W/cm^2. Differences can be explained by differences in skull thickness and densities in the animal models.

These results, along with sonication-related pain that occurred in patient number two, suggest that the safety window appears to be relatively narrow and could limit the extent of the brain that can be targeted with this device without overheating the skull. The locations of these patients' tumors, relatively deep and centrally located, were nearly optimal for this device with respect to skull heating. Such locations allow the ultrasound beam to be distributed over a large portion of the skull and result in nearly normal angles between most of the array elements and the skull. For tumors that are not centered in this way, the angles between the skull bone and the transducer face would deviate from normal, resulting in nearly complete reflection for many elements. Deactivation of those elements would result in a smaller portion of the transducer surface being active and higher local ultrasound intensities on the skull. Despite these limitations, the device appears to be capable of noninvasively ablating deep and centrally

located tumors, locations where surgery is challenging or not an option. It may also be useful for noninvasive functional neurosurgery, where many targets are deep within the brain. The source of the sonication-related pain in one patient is not known. We suspect that the pain resulted from heating of the dura. It is possible that the dura extended into the brain midline in this patient and was perhaps close to the focal zone.

To improve the targetable locations in the brain, the manufacturer has made substantial changes to the device and treatment strategy to be used subsequent patient treatments in this trial (38). These changes include doubling the number of elements in the phased array, increasing the maximum available power, lowering the ultrasound frequency, taking advantage of bubble-enhanced absorption to boost the focal heating (46). The thermoplastic mask has also been replaced by a standard stereotactic surgery device with pins to prevent motion and discomfort. This motion resulted in long treatments (due to a need to repeat the treatment planning) and may have caused error in the aberration correction and in the MRTI. Results of treatments with this new version of the TcMRgFUS system will be presented separately.

We should note that several factors potentially resulted in an underestimation of the ratio of focus to brain surface heating. Because the design of this prototype device precluded the use of an imaging coil, the body coil was used for the imaging, and a 3-5 mm slice thickness was necessary to achieve marginally acceptable MRTI. Volume averaging (i.e. the partial volume effect), especially if the focal spot was not centered on the slice, likely resulted in an underestimation of the maximum temperature achieved. In addition, the small patient motion that was observed over the course of the treatment could have degraded the aberration correction, resulting in suboptimal focusing. Furthermore, our method to conservatively estimate the brain surface heating was susceptible to some bias resulting from noise and/or phase instabilities that were not corrected, potentially resulting in an overestimate of the skull-induced heating. Finally, it could be possible that the cooling of the scalp during treatment could actually drop the brain surface temperature, which would increase the safety window.

A major limitation of the study was our inability to achieve ablation in these patients. Prior tests with this device sonicating in vivo tissue in rabbits through a human skull sample were able to create thermal lesions. In that study, focal temperature changes of 22 ± 10°C/kW were achieved (25), which was larger than the average value of 15.5 ± 5.1°C/kW in these treatments. This difference was likely due to the human treatments being at deeper tissue locations and the difference between ultrasound absorption and blood perfusion in the normal rabbit brain and human tumors. We may have been able to achieve ablation in our patients if we had used longer sonications or performed additional sonications to accumulate the thermal dose past the damage threshold at the focal spot. However, due to long treatment times, patient discomfort due to the thermoplastic mask, and our desire to be conservative in these first treatments, such additional exposures were not attempted.

Another limitation of this study was the quality of the MRTI. The noise level was only acceptable using a 3-5 mm slice thickness, and it increased during sonication. Future device designs would benefit greatly from integration of an imaging coil to allow for multiple, thinner images planes with better in plane resolution for the MRTI and from better electrical isolation of the TcMRgFUS hardware to reduce sonication-related noise. The large phase instabilities observed in the MRTI were also problematic. While similar artifacts have been reported in other works resulting from patient motion or magnetic field instabilities, we did not expect them to occur in the brain with this system, where the head is fixed in place. The source of these instabilities, while not clear, were potentially due to magnetic field changes due to blood flow or brain pulsation, or more likely, motion of the mouth and tongue or other body parts outside of the brain during sonication. We do not suspect that they were produced by the TcMRgFUS system (such as from water motion) or from instabilities in the MRI itself, as they

were not observed in preclinical tests with this device (15,15,25,27,27). Our correction algorithm appeared to successfully remove the phase instabilities overall, but future work will be needed to validate it. While analysis of the method using dummy (non-targeted) locations suggests that it can robustly correct errors in ROI's within the brain, sometimes the instabilities appeared to remain after correction at the brain surface. This might be expected, as the extrapolation of the fit surface of the artifact at the edges is based on less information than at ROI's within the brain that are completely surrounded.

An additional problem occurred in patient number three, where signal loss in the MRTI, presumably resulting from blood products remaining from a prior intervention, prevented us from mapping the temperature changes in a substantial portion of that tumor. This loss was presumably to T2* shortening due to magnetic susceptibility differences. If methods cannot be developed to compensate for such artifacts, they could pose a limitation to this technology in these cases. In particular, many high grade gliomas as well as melanoma and renal cell carcinoma metastases have such blood products that may cause difficulty with the MRTI.

Conclusion

This work has shown for the first time that ultrasound can be focused through the intact skull in patients, and that the heating can be visualized using MR temperature imaging. While device power limited our ability to achieve thermal coagulation, extrapolation of the results suggests that ablation will be possible without overheating the skull. Analysis of the brain surface heating and the occurrence of sonication-related pain in one patient suggests, however, that the targetable regions of the brain may be limited to deep, central locations in the brain with the device.

Acknowledgments

The authors would like extend their gratitude to Eyal Zadicario, Joanne O'Hara, Jason White, and Kevin Lanctot for their help with these treatments. This study was supported by NIH Grant R01EB003268. InSightec funded the clinical trial. The authors have no financial interest or conflicts of interest for this work. Two authors (KH and FAJ) served in the past as consultants for InSightec. The author that performed the analysis (NM) had full control of the data gathered in the study.

This study was supported by NIH Grant R01EB003268. InSightec funded the clinical trial.

Reference List

1. Anzai Y, Lufkin R, DeSalles A, Hamilton DR, Farahani K, Black KL. Preliminary experience with MR-guided thermal ablation of brain tumors. AJNR Am J Neuroradiol 1995;16:39–48. [PubMed: 7900601]
2. Astrom KE, Belle, Ballantine HT, Heidensleben E. An experimental neuropathological study of the effects of high-frequency focused ultrasound on the brain of the cat. J Neuropathol Exp Neurol 1961;20:484–520. [PubMed: 13684889]
3. Aubry JF, Tanter M, Pernot M, Thomas JL, Fink M. Experimental demonstration of noninvasive transskull adaptive focusing based on prior computed tomography scans. J Acoust Soc Am 2003;113:84–93. [PubMed: 12558249]
4. Ballantine HT, Hueter TF, NAUTA WJ, SOSA DM. Focal destruction of nervous tissue by focused ultrasound: biophysical factors influencing its application. J Exp Med 1956;104:337–360. [PubMed: 13357689]
5. Barnard JW, Fry WJ, Fry FJ, Krumins RF. Effects of high intensity ultrasound on the central nervous system of the cat. J Comp Neurol 1955;103:459–484. [PubMed: 13286367]
6. Berg AT. Are febrile seizures provoked by a rapid rise in temperature? Am J Dis Child 1993;147:1101–1103. [PubMed: 8213683]

7. Capek, M.; Mroz, L.; Wegenkittl, R. Robust and Fast Medical Registration of 3D-Multi-Modality Data Sets. Proc.Medicon 2001 (IX Mediterranean Conference on Medical and Biological Engineering and Computing); 2001. p. 515-518.
8. Chapelon JY, Ribault M, Vernier F, Souchon R, Gelet A. Treatment of localised prostate cancer with transrectal high intensity focused ultrasound. Eur J Ultrasound 1999;9:31–38. [PubMed: 10099164]
9. Clement GT, Hynynen K. A non-invasive method for focusing ultrasound through the human skull. Phys Med Biol 2002;47:1219–1236. [PubMed: 12030552]
10. Clement GT, Hynynen K. Correlation of ultrasound phase with physical skull properties. Ultrasound Med Biol 2002;28:617–624. [PubMed: 12079698]
11. Clement GT, Hynynen K. Micro-receiver guided transcranial beam steering. IEEE Trans Ultrason Ferroelectr Freq Contr 2002;49:447–453.
12. Clement GT, Sun J, Giesecke T, Hynynen K. A hemisphere array for non-invasive ultrasound brain therapy and surgery. Phys Med Biol 2000;45:3707–3719. [PubMed: 11131194]
13. Clement GT, White J, Hynynen K. Investigation of a large-area phased array for focused ultrasound surgery through the skull. Phys Med Biol 2000;45:1071–1083. [PubMed: 10795992]
14. Clement GT, White PJ, Hynynen K. Enhanced ultrasound transmission through the human skull using shear mode conversion. J Acoust Soc Am 2004;115:1356–1364. [PubMed: 15058357]
15. Clement GT, White PJ, King RL, McDannold N, Hynynen K. A Magnetic Resonance Imaging-Compatible, Large-Scale Array for Trans-Skull Ultrasound Surgery and Therapy. J Ultrasound Med 2005;24:1117–1125. [PubMed: 16040827]
16. Connor CW, Clement GT, Hynynen K. A unified model for the speed of sound in cranial bone based on genetic algorithm optimization. Phys Med Biol 2002;47:3925–3944. [PubMed: 12476974]
17. el Radhi AS, Banajeh S. Effect of fever on recurrence rate of febrile convulsions. Arch Dis Child 1989;64:869–870. [PubMed: 2774621]
18. Fry FJ, Goss SA. Further studies of the transkull transmission of an intense focused ultrasonic beam: lesion production at 500 kHz. Ultrasound Med Biol 1980;6:33–38. [PubMed: 7368418]
19. Fry WJ, Brennan JF, Barnard JW. Histological study of changes produced by ultrasound in the gray and white matter of the central nervous system. Ultrasound Med Biol 1957;3:110–130.
20. Guthkelch AN, Carter LP, Cassady JR, Hynynen K, Iacono RP, Johnson PC, Obbens EA, Roemer RB, Seeger JF, Shimm DS. Treatment of malignant brain tumors with focused ultrasound hyperthermia and radiation: results of a phase I trial. J Neurooncol 1991;10:271–284. [PubMed: 1654406]
21. Heimburger RF. Ultrasound augmentation of central nervous system tumor therapy. Indiana Med 1985;78:469–476. [PubMed: 4020091]
22. Hickey RC, Fry WJ, Meyers R, Fry FJ, BRADBURY JT. Human pituitary irradiation with focused ultrasound. An initial report on effect in advanced breast cancer. Arch Surg 1961;83:620–633. [PubMed: 13907178]
23. Hindman JC. Proton resonance shift of water in the gas and liquid states. J Chem Phys 1966;44:4582–4592.
24. Hynynen K. The role of nonlinear ultrasound propagation during hyperthermia treatments. Med Phys 1991;18:1156–1163. [PubMed: 1753899]
25. Hynynen K, Clement GT, McDannold N, Vykhodtseva N, King R, White PJ, Vitek S, Jolesz FA. 500-element ultrasound phased array system for noninvasive focal surgery of the brain: A preliminary rabbit study with ex vivo human skulls. Magn Reson Med 2004;52:100–107. [PubMed: 15236372]
26. Hynynen K, Jolesz FA. Demonstration of potential noninvasive ultrasound brain therapy through an intact skull. Ultrasound Med Biol 1998;24:275–283. [PubMed: 9550186]
27. Hynynen K, McDannold N, Clement G, Jolesz FA, Zadicario E, Killiany R, Moore T, Rosen D. Pre-clinical testing of a phased array ultrasound system for MRI-guided noninvasive surgery of the brain-A primate study. Eur J Radiol. 2006
28. Hynynen K, Vykhodtseva NI, Chung AH, Sorrentino V, Colucci V, Jolesz FA. Thermal effects of focused ultrasound on the brain: determination with MR imaging. Radiology 1997;204:247–253. [PubMed: 9205255]

29. Ishihara Y, Calderon A, Watanabe H, Okamoto K, Suzuki Y, Kuroda K. A precise and fast temperature mapping using water proton chemical shift. Magn Reson Med 1995;34:814–823. [PubMed: 8598808]
30. Jolesz FA, Bleier AR, Jakab P, Ruenzel PW, Huttl K, Jako GJ. MR imaging of laser-tissue interactions. Radiology 1988;168:249–253. [PubMed: 3380968]
31. Kahn T, Bettag M, Ulrich F, Schwarzmaier HJ, Schober R, Furst G, Modder U. MRI-guided laser-induced interstitial thermotherapy of cerebral neoplasms. J Comput Assist Tomogr 1994;18:519–532. [PubMed: 8040431]
32. Kettenbach J, Kuroda K, Hata N, Morrison PR, McDannold NJ, Gering P, Saiviroonporn P, Zientara GP, Mc Black PL, Kikinis R, Jolesz FA. Laser-induced thermotherapy of cerebral neoplasia under MR tomographic control. Min Invas Ther & Allied Technol 1998;7:589–598.
33. Lele PP. A simple method for production of trackless focal lesions with focused ultrasound: Physical factors. J Physiol 1962;160:494–512. [PubMed: 14463953]
34. Lynn JG, Zwemer RL, Chick AJ, Miller AE. A new method for the generation and use of focused ultrasound in experimental biology. J Gen Physiol 1942;26:179–193. [PubMed: 19873337]
35. Lyons BE, Obana WG, Borcich JK, Kleinman R, Singh D, Britt RH. Chronic histological effects of ultrasonic hyperthermia on normal feline brain tissue. Radiat Res 1986;106:234–251. [PubMed: 3704114]
36. McDannold N, King RL, Hynynen K. MRI monitoring of heating produced by ultrasound absorption in the skull: in vivo study in pigs. Magn Reson Med 2004;51:1061–1065. [PubMed: 15122691]
37. McDannold N, Vykhodtseva N, Jolesz FA, Hynynen K. MRI investigation of the threshold for thermally induced blood-brain barrier disruption and brain tissue damage in the rabbit brain. Magn Reson Med 2004;51:913–923. [PubMed: 15122673]
38. McDannold, N.; Zadicario, E.; Pilatou, MC.; Jolesz, FA. Preclinical testing of a second-generation MRI-guided focused ultrasound system for transcranial brain tumor ablation. 16th Scientific Meeting, International Society for Magnetic Resonance in Medicine; Toronto, Canada. 2008.
39. Meshorer A, Prionas SD, Fajardo LF, Meyer JL, Hahn GM, Martinez AA. The effects of hyperthermia on normal mesenchymal tissues. Application of a histologic grading system. Arch Pathol Lab Med 1983;107:328–334. [PubMed: 6687797]
40. Meyers R, Fry WJ, Fry FJ, Dreyer LL, Schultz DF, Noyes RF. Early experiences with ultrasonic irradiation of the pallidfugal and nigral complexes in hyperkinetic and hypertonic disorders. J Neurosurg 1959;16:32–54. [PubMed: 13621264]
41. Oka M, Okumura T, Yokoi H, Murao T, Miyashita Y, Oka K, Yoshitatsu S, Yoshioka K, Hirano H, Kawashima Y. Surgical application of high intensity focused ultrasound. Med J Osaka Univ 1960;10:427–442.
42. Park, JW.; Jung, S.; Junt, TY.; Lee, MC. Focused ultrasound surgery for the treatment of recurrent anaplastic astrocytoma: A preliminary report. Therapeutic Ultrasound.5th International Symposium on Therapeutic Ultrasound; 2006. p. 238-240.
43. Ram Z, Cohen ZR, Harnof S, Tal S, Faibel M, Nass D, Maier SE, Hadani M, Mardor Y. Magnetic resonance imaging-guided, high-intensity focused ultrasound for brain tumor therapy. Neurosurgery 2006;59:949–955. [PubMed: 17143231]
44. Sanghvi NT, Foster RS, Bihrle R, Casey R, Uchida T, Phillips MH, Syrus J, Zaitsev AV, Marich KW, Fry FJ. Noninvasive surgery of prostate tissue by high intensity focused ultrasound: an updated report. Eur J Ultrasound 1999;9:19–29. [PubMed: 10099163]
45. Sapareto SA, Dewey WC. Thermal dose determination in cancer therapy. Int J Radiat Oncol Biol Phys 1984;10:787–800. [PubMed: 6547421]
46. Sokka SD, King R, Hynynen K. MRI-guided gas bubble enhanced ultrasound heating in in vivo rabbit thigh. Phys Med Biol 2003;48:223–241. [PubMed: 12587906]
47. Sun J, Hynynen K. The potential of transskull ultrasound therapy and surgery using the maximum available skull surface area. J Acoust Soc Am 1999;105:2519–2527. [PubMed: 10212433]
48. Tempany CM, Stewart EA, McDannold N, Quade BJ, Jolesz FA, Hynynen K. MR Imaging-guided focused ultrasound surgery of uterine leiomyomas: a feasibility study. Radiology 2003;226:897–905. [PubMed: 12616023]

49. Thomas J, Fink MA. Ultrasonic beam focusing through tissue inhomogeneities with a time reversal mirror: applicaton to transskull therapy. IEEE Trans Ultrason Ferroelectr Freq Contr 1996;43:1122–1129.
50. Vykhodtseva NI, Gavrilov LR, Mering TA, Iamshchikova NG. [Use of focused ultrasound for local destruction of different brain structures] Primenenie fokusirovannogo ul'trazvuka dlia lokal'nykh razrushenii razlichnykh struktur golovnogo mozga. Zh Nevropatol Psikhiatr 1976;76:1810–1816. [PubMed: 797196]
51. Vykhodtseva NI, Sorrentino V, Jolesz FA, Bronson RT, Hynynen K. MRI detection of the thermal effects of focused ultrasound on the brain. Ultrasound Med Biol 2000;26:871–880. [PubMed: 10942834]
52. Warwick R, Pond J. Trackless lesions in nervous tissues produced by high intensity focused ultrasound (high-frequency mechanical waves). J Anat 1968;102:387–405. [PubMed: 4968493]
53. Wu F, Chen WZ, Bai J, Zou JZ, Wang ZL, Zhu H, Wang ZB. Pathological changes in human malignant carcinoma treated with high-intensity focused ultrasound. Ultrasound Med Biol 2001;27:1099–1106. [PubMed: 11527596]

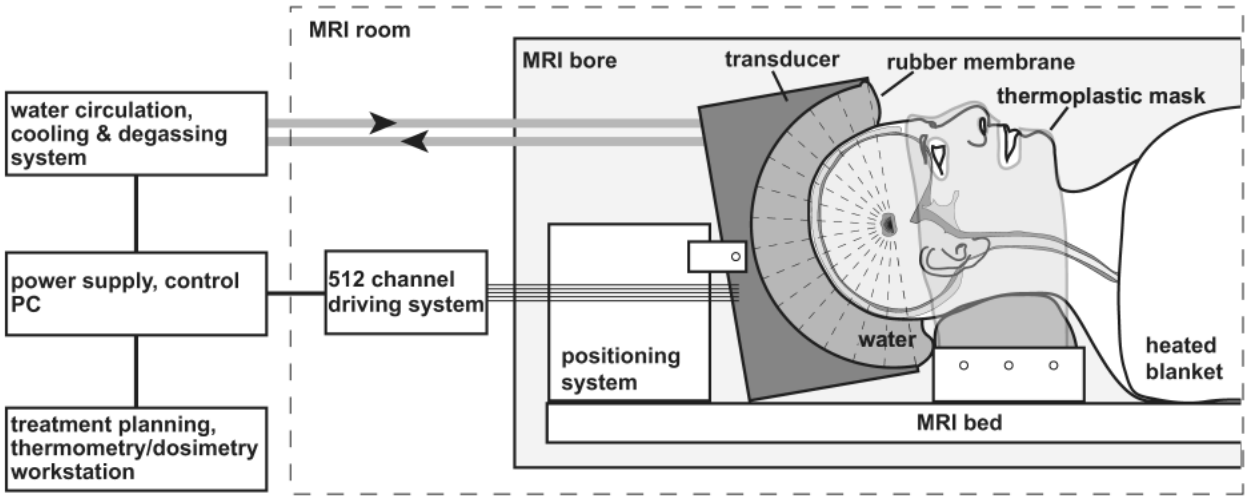

Figure 1.
Diagram of the TcMRgFUS device for noninvasive brain tumor ablation.

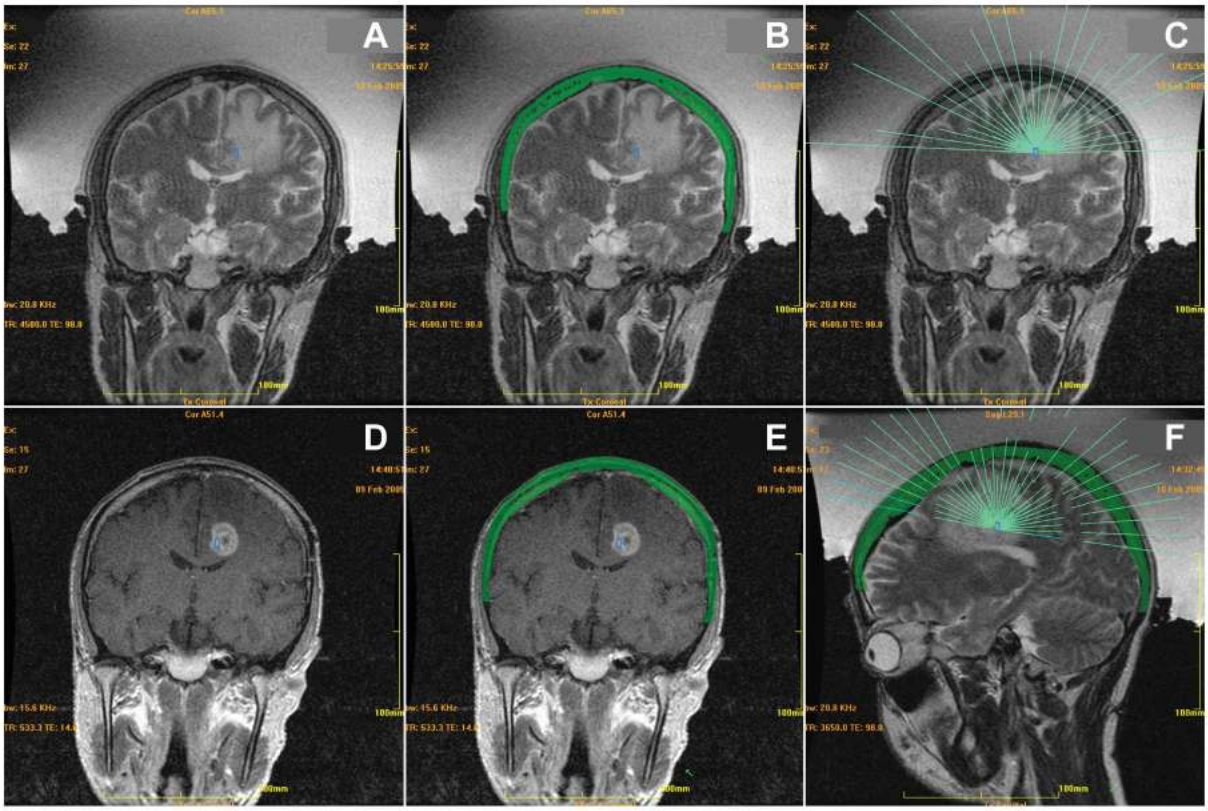

Figure 2.

Screenshots from TcMRgFUS treatment planning workstation. **(A)** Coronal T2-weighted images of the patient in the TcMRgFUS device. The target of the current sonication is indicated by the blue rectangle. The water filling the space between the patient's shaved head and the transducer can be seen. **(B)** Pre-treatment CT scan data of the skull is registered the intra-treatment MRI scans. The skull is automatically segmented from the CT scan and displayed on top of the MRI images used for treatment planning as a green region. Any registration errors can be seen on these images and corrected by the user using a graphical tool. MR tracking coils integrated into the transducer are used to register the TcMRgFUS system coordinates with the imaging coordinates. Acoustic models taking into account the patient-specific skull geometry and density are used to correct for aberrations to the ultrasound beam. **(C)** The beam paths for each phased array element are superimposed on the images, allowing the user to verify that no beams pass through undesired structures. **(D)-(E)**. Pre-treatment contrast-enhanced T1-weighted images, which can be useful to define tumor margins, acquired the day before treatment can also be registered to the intra-treatment images. Axial and sagittal images are also acquired, allowing for treatment planning in three dimensions. **(F)**. Sagittal T2-weighted image.

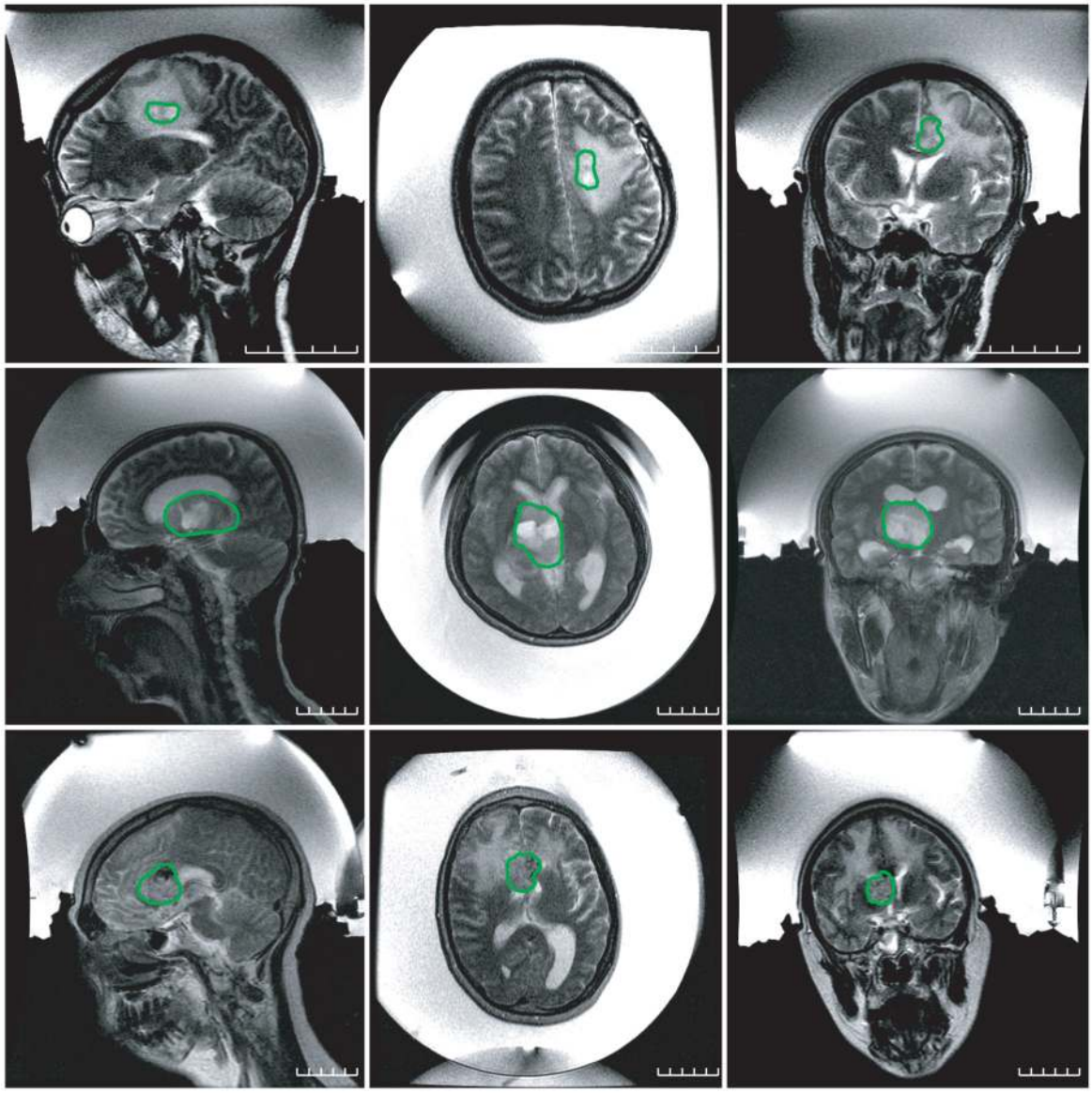

Figure 3.
T2-weighted FSE images of the patients within the TcMRgFUS device. The outlines approximately delineate the boundaries of the targeted tumors. The space between the patients' shaved heads and the hemispherical transducer was filled with chilled water that was continuously degassed and circulated before and between sonications. (Top: patient #1, middle: patient #2, right: patient #3; left: sagittal images, center: axial images, right: coronal images)

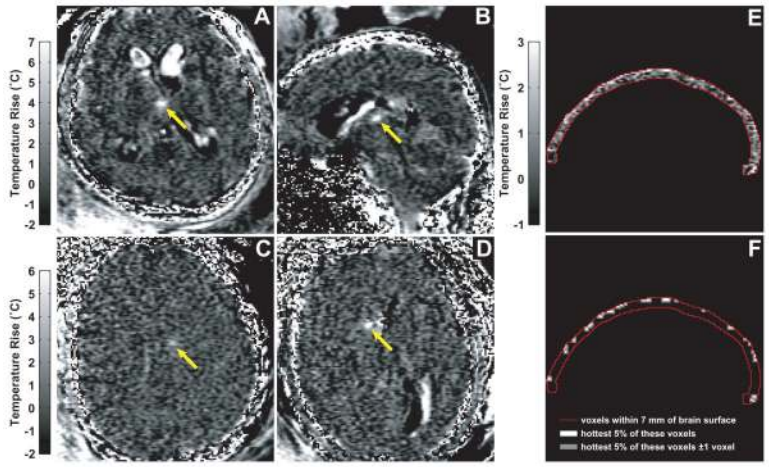

Figure 4.

(A)-(D) Focal heating during TcMRgFUS in the three patients. **(A)-(B):** Sagittal **(A)** and axial **(B)** examples of MRTI acquired at peak temperature rise during two 20 s sonications (acoustic power: 800 W) in patient number two. **(C)-(D):** Axial MRTI showing focal heating in patients one and three, respectively (acoustic power: 650W, 594W). The focus in patient three was located close to a region containing blood products from a prior biopsy, which caused signal loss and artifact in the MRTI. Flow of the fluid in the ventricles produced phase instabilities that resulted in the white and black areas evident in the brain away from the focal spot that can be seen in A, B, and D. Images shown at native resolution. Areas with low magnitude signal produced white noise in the phase-difference images used for MRTI that are evident in the skull bone and at image periphery **(E):** Heating on the brain surface by the acoustic absorption in the skull, at the end of the MRTI acquisition resulting from a 20 s sonication in patient number 3 (acoustic power: 491 W). The heating was quantified by searching for the hottest voxels in the displayed 6-7 voxel wide strip in a composite image that was the average of three or more temperature maps acquired when the brain surface temperature was at steady state. **(E)** The location of the hottest 5% of the voxels in this strip ±1 voxel that were used to provide a conservative estimate of the brain surface heating.

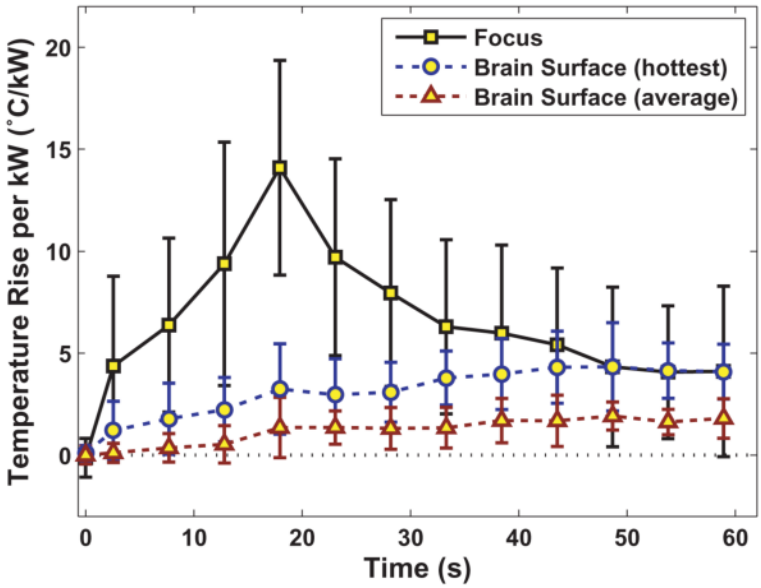

Figure 5.

Temperature rise normalized to the applied acoustic power as a function of time at the focus and on the brain surface as measured by MRTI. The brain surface was heated by the skull bone, which is highly absorbing of ultrasound. Two metrics were tested to measure the temperature on the brain surface. The first aimed to be a conservative (worse-case) metric that identified any hot spots at particular locations and considered the hottest voxels within 6-7 voxels of the brain surface. The second measured the mean temperature rise of all voxels within a two voxel wide strip at the brain surface. Mean ± standard deviation shown of 28 sonications for focal heating, 15 for brain surface heating. The data showing the temperature at the focus is from all sonications in the three patients where focal heating was observed in MRTI; the brain surface heating was from all sonications in the three patients where sagittal or coronal MRTI was used.

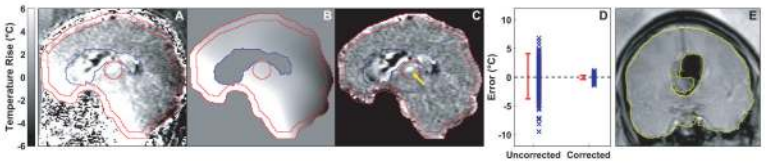

Figure 6.

Artifacts in the MRTI. **(A)** Instabilities in the phase-difference images caused artifacts seen as apparent temperature changes in MRTI that were clearly not related to the sonications. Non-heated regions in the brain – the entire brain in the image except for an outer strip at the brain surface and a one cm ROI centered on the focal spot – were used to remove these artifacts. The ventricles (blue segmentation) were also excluded because they contained uncorrelated phase artifacts, presumably related to fluid flow caused by acoustic streaming. **(B)** The phase-difference in the non-heated regions were fit to a smooth surface and extrapolated into the heated regions. **(C)** This surface was then subtracted from the phase-difference image. **(D)** This correction was tested by repeating the procedure using an ROI in a non-heated brain area instead of that surrounding the focal point and verifying that after correction the mean apparent temperature change was zero. The plot shows temperature error in these ROI's in all of the individual temperature maps acquired during all of the 45 sonications before and after the correction. **(E)** In patient number three, a large signal void in the images used to create the MRTI prevented temperature measurement in a large proportion of the tumor. The magnitude reconstruction of the gradient echo sequence used for MRTI is shown.